Chemistry Europe
European Chemical Societies Publishing

WILEY VCH

Excellence in Chemistry Research

Announcing our new flagship journal

- Gold Open Access
- Publishing charges waived
- Preprints welcome
- Edited by active scientists

Meet the Editors of *ChemistryEurope*

Luisa De Cola
Università degli Studi di Milano Statale, Italy

Ive Hermans
University of Wisconsin-Madison, USA

Ken Tanaka
Tokyo Institute of Technology, Japan

ChemistrySelect

Research Article
doi.org/10.1002/slct.202302560

Chemistry Europe
European Chemical Societies Publishing

www.chemistryselect.org

Simple Disulfides: Studies of Some Exponents of a Family Involved in Prominent Processes

Vanina M. Cayón,[a] Mauricio F. Erben,*[a] Rosana M. Romano,[a] Hans-Georg Stammler,[b] Norbert W. Mitzel,*[b] Mao Fa Ge,[c] and Carlos O. Della Védova*[a]

Exploring the fundamental chemistry and intrinsic properties of disulfide-containing species has become an increasingly popular means to understand their action in various scientific fields, applications, and systems. In this study several representatives of this extensive family with the general formula CCl_3SSR, where R represents CH_2CH_3, CH_2CF_3, $C(CH_3)_3$, C_6H_5 and $C(O)CH_3$,were prepared and characterized by vibrational spectroscopy methods (FTIR and Raman), NMR spectroscopy, mass spectrometry, X-ray structure determinations and photo electron spectroscopy. When complemented with computational chemistry, this range of methods and techniques sheds new light on numerous different processes. It is worth noting that the importance in disulfides compounds is related to inherent properties of this chemical family, such as chirality, theories involving the origin of life and its evolution, and, lately, the mechanisms of S–S bond formation in processes concerning therapies based on the use of peptides and COVID-19.

Introduction

The simplest disulfide, H_2S_2, was discovered by Carl Wilhelm Scheele in 1777 as part of his 15000 to 20000 experiments documented in his laboratory notes.[1] This huge number of experiments conducted by Scheele is a testament to his endless curiosity as a chemist. In addition to H_2S_2, Scheele independently discovered chemical elements such as oxygen, chlorine, barium, molybdenum, tungsten and manganese.

H_2S_2 adopts C_2 symmetry with a dihedral angle of 88.68°. Its non-hybridized sulfur character can be deduced by comparing it to H_2O_2, which has a torsion angle of 113.70°.[2] The singular geometry of H_2S_2 results in non-superimposable mirror images. Its isotopologue D_2S_2 was used to calculate a tunneling period of 5.6 milliseconds at room temperature and a helium pressure of 1.6×10^{-5} bar.[3,4] This implies that if both D_2S_2 enantiomers were to travel the same distance in high vacuum, they would undergo a randomization process resulting in an equal concentration of both optical isomers. However, at higher helium pressures, the final composition would be different as He stabilizes a particular chiral state. This experiment with D_2S_2 is more convenient than using H_2S_2 since the lighter isotopologue presents a faster tunneling time.

Simple species, light, and chirality are key factors that provide insights into the origin of life in the primeval universe. Simple and small molecules were the first stations on the path towards more complex organic species and the origin of life. There are various hypotheses, some of which are controversial, that aim to reveal this origin. In his theory, Wächtershäuser considers disulfides as the primary energy source, and pyrite (FeS_2), which exists in the marine interface, played a key role as template in the fixation of carbon compounds. This led him to propose the "iron-sulfide world hypothesis" for the origin of life.[5] He proposed that pyrite could work catalytically to give bifunctional C2 and C3-organic structures of a proto-nucleic acid, which could be considered a pioneer organism. This pioneer organism could then react further to form larger biocompounds such as proteins, leading to a gradual increase in complexity and eventually producing nucleic acids. Kundell suggests that the previously proposed evolutionary process could be significantly shortened and simplified by using pyrite directly to produce protonucleic acid.[6]

Disulfide bonds play a crucial role in the formation of proteins and peptides. For instance, in the case of simple amino acids such as cysteine, the process of disulfide formation involves the stabilization of a tertiary structure through the formation of an intramolecular S–S bridge. This occurs when

[a] Dr. V. M. Cayón, Prof. Dr. M. F. Erben, Prof. Dr. R. M. Romano, Prof. Dr. C. O. Della Védova
CEQUINOR (UNLP-CONICET, CCT-La Plata, associated with CIC),
Departamento de Química, Facultad de Ciencias Exactas,
Universidad Nacional de La Plata,
Boulevard 120 e/60 y 64 N°1465 La Plata
B1900, Buenos Aires, Argentina
E-mail: erben@quimica.unlp.edu.ar
carlosdv@quimica.unlp.edu.ar

[b] Dr. H.-G. Stammler, Prof. Dr. N. W. Mitzel
Universität Bielefeld,
Lehrstuhl für Anorganische Chemie und Strukturchemie,
Universitätsstraße 25,
33615 Bielefeld,
Germany
E-mail: mitzel@uni-bielefeld.de

[c] Prof. Dr. M. Fa Ge
State Key Laboratory for Structural Chemistry of Unstable and Stable Species, Institute of Chemistry, Chinese Academy of Sciences,
Beijing 100190,
China

Supporting information for this article is available on the WWW under https://doi.org/10.1002/slct.202302560

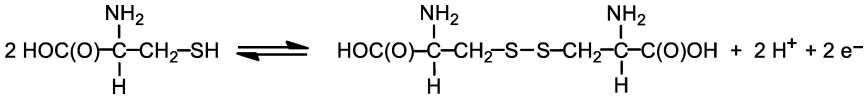

Scheme 1. Intramolecular disulfide bond formation in the cysteine-cystine system.

the thiol form undergoes oxidative evolution to give the disulfide species, as represented by the following equilibrium (Scheme 1).

In extracellular fluid where thiol and disulfide forms coexist, the ratio between the concentration of thiols (C_{SH}) and that of disulfides (C_{SS}) is dependent on the nature of the medium. In a reductive environment, the C_{SH}/C_{SS} ratio increases, resulting in a relatively greater amount of reduced thiol form, while in an oxidative environment, the form with disulfide bonds increases, causing a decrease in the C_{SH}/C_{SS} ratio. This oxidative condition is precisely what occurs during the aging process. The oxidative characteristics of an extracellular environment facilitate the physical interactions between viral proteins and cell surface receptors, followed by membrane fusion and virus internalization. Although there is some agreement that disulfide bonds have been generated evolutionarily to improve the stability of proteins by stabilizing them in their molecular environment, recent evidence would indicate that the cleavage of one or more of their bonds is controlled by catalysts facilitators that are specific for their specific substrate.[7] More recently, disulfide bonds were studied as restricted elements with additional implications for the development of therapies based on the use of peptides. For this, versatile functions of disulfide bonds formed between cysteine residues in therapeutic peptides have been considered.[8]

The behavior of disulfides can be understood by examining results obtained from simpler examples. Therefore, this work presents the preparation of a new disulfide compound, $CCl_3SSCH_2CF_3$, along with known species. The results, including those obtained using Photoelectron Spectroscopy (PES), will be presented in a comparative context that includes relevant data from the literature. Additionally, NMR data, mass, vibrational, and X-ray spectra for the species $CCl_3SSC(CH_3)_3$ will be presented as part of a study of a series of disulfides. This series can be summarized asCCl_3SSR (R=CH_2CH_3, CH_2CF_3, $C(CH_3)_3$, C_6H_5, $C(O)CH_3$).

Experimental Section

Synthesis

CAUTION: Perchloromethylmercaptan, CCl_3SCl, is a highly toxic, corrosive and odorous substance, both by contact and by inhalation. It causes severe skin burns and is highly irritating and obstructive to the respiratory tract. It must be handled in conditions consistent with these properties ensuring adequate ventilation, especially in confined areas. In this work, manometric vacuum techniques were used for its manipulation under an extraction hood and security procedures were taken to avoid and minimize any possible contact with the substance.

Trichloromethyl disulfides CCl_3SSR (R=CH_2CH_3, CH_2CF_3, $C(CH_3)_3$, C_6H_5, $C(O)CH_3$) are obtained using the following general reaction (Scheme 2).[9,10]

The progress of the reaction can be monitored by observing the vanishing of the intense yellow color of perchloromethylmercaptan. This compound is transformed into a pale yellow or colorless substance, which results from the formation of a disulfide reaction product.

Ethyltrichloromethyl disulfide, $CCl_3SSCH_2CH_3$: In a reaction tube equipped with a Young's stopcock connected to a vacuum line, 8 mmol of ethanethiol was condensed onto the stoichiometric amount of CCl_3SCl. When stirred in a cold bath, bubbles appeared and the solution discolored. The resulting mixture was then distilled under reduced pressure and a colorless liquid substance was observed in the −40 °C bath after trap-to-trap distillation.

Trifluoroethyltrichloromethyl disulfide, $CCl_3SSCH_2CF_3$: The procedure was similar to before, except that the reaction time was extended to 48 h. After trap-to-trap distillation, a colorless liquid was obtained in the trap at −40 °C.

Tert-butyl trichloromethyl disulfide, $CCl_3SSC(CH_3)_3$: 12 mmol of CCl_3SCl were condensed onto the stoichiometric amount of *tert*-butylthiol and the mixture was allowed to react at room temperature. Afterward, a colorless liquid was obtained in the trap at −40° C.

Trichloromethyl phenyl disulfide, $CCl_3SSC_6H_5$: In a cold bath at −20 °C, 12 mmol of thiophenol was condensed onto the stoichiometric amount of CCl_3SCl. After 72 h, the reaction was complete, as evidenced by the presence of bubbles and discoloration in the solution. The product was then distilled under reduced pressure to remove hydrogen chloride, and the desired product was collected in a −40 °C bath. The resulting liquid product is colorless at room temperature.

Acetyltrichloromethyl disulfide, $CCl_3SSC(O)CH_3$: In a 100 mL Schlenk flask at −30 °C, 24 mmol of thioacetic acid was added. An equimolar amount of CCl_3SCl was slowly added and allowed to slowly reach room temperature. The reaction was instantaneous, as evidenced by the discoloration of the solution. The reaction product was then distilled under reduced pressure and collected in the −40 °C bath. The resulting liquid substance shows a slight yellowish color at room temperature

^1H, ^{13}C and ^{19}F NMR spectra

The ^1H, ^{13}C and ^{19}F NMR spectra were recorded using Bruker AV 300 NMR spectrometer.Table 1 displays the ^1H, ^{13}C and ^{19}F NMR signals of the CCl_3SSR (R=CH_2CH_3, CH_2CF_3, $C(CH_3)_3$, C_6H_5, $C(O)CH_3$) family obtained at 298 K using 5 mm probes and $CDCl_3$ as the lock.

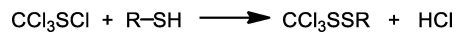

Scheme 2. Chemical reaction to obtaintrichloromethyldisulfides compounds.

Table 1. ^{1}H, ^{13}C and ^{19}F NMR chemical shifts of the species CCl_3SSR and CCl_3SR (R=CH_2CH_3, CH_2CF_3, $C(CH_3)_3$, C_6H_5, $C(O)CH_3$). Calculated ^{13}C NMR and ^{1}H NMR shifts are bold highlighted.[11–13]

CCl_3SSR[a]	$\delta^{1}H$ [ppm]	$\delta^{13}C$ [ppm]	$\delta^{19}F$ [ppm]	$\delta^{13}C$ [ppm] CCl_3SR[a]
CH_2CH_3	1.4 (t, J=7.5 Hz, 3H)/**1.07**	101.4 (CCl_3)/**99.2**	–	**102.9**
	3.1 (q, J=7.0 Hz, 2H)/**3.04**	33.8 ($C^{\beta}H_2$)/**32.8**		**25.6**
		14.4 ($C^{\alpha}H_3$)/**14.5**		**14.7**
CH_2CF_3	3.7 (q, J=9.0 Hz, 2H)/**3.40**	125.1 ($C^{\alpha}F_3$, q, $^{1}J_{FC}$=274.6 Hz)/**125.2**	−66.5	**125.2**
		103.5 (CCl_3)/**99.2**		**102.9**
		42.0 ($C^{\beta}H_2$, q, $^{2}J_{FC}$=32.2 Hz)/**33.6**		**33.6**
$C(CH_3)_3$	1.5 (s, 9H)/**1.27**	100.2 (CCl_3)/**99.2**	–	**102.9**
		50.1 (C^{β})/**45.6**		**47.8**
		31.1 (C^{α})/**30.5**		**30.7**
C_6H_5	7.7 (m, 2H)/**7.24**	134.9 (C^{i})/**135.0**	–	**132.9**
	7.4 (m, 3H)/**7.24**	129.7 (C^{α})/**129.0**		**131.3**
		129.3 (C3)/**128.5**		**128.5**
		128.6 (C4)/**127.8**		**127.8**
		100.6 (CCl_3)/**99.2**		**102.9**
$C(O)CH_3$	2.6 (s)/**2.15**	189.4 (C=O)/**192.2**	–	**194.5**
		99.3 (CCl_3)/**99.2**		**102.9**
		28.9 ($C^{\beta}H_3$)/**28.7**		**30.2**

[a] CCl_3S–S–C^{β}–$C^{\alpha}$and CCl_3S–C^{β}–C^{α} units.

Photoionization mass spectra (PIMS) and photoelectron spectra /PES)

The double chamber UPS-II machine used for the study of the CCl_3SSR (R=CH_2CH_3, CH_2CF_3, $C(CH_3)_3$, C_6H_5, $C(O)CH_3$) series is designed to detect transient species with a high resolution of about 30 meV, as indicated by the spin-orbit splitting of $Ar^{+}(^{2}P_{3/2}, ^{2}P_{1/2})$ photoelectron signals.[14] Experimental vertical ionization energies (IP in eV) were calibrated by simultaneous addition of a small amount of argon and methyl iodide to the sample. The ionization source used in the experiment is single-wavelength HeI radiation of 21.21 eV.

Although PE and PIMS spectra are not measured simultaneously, they are recorded within seconds of each other under identical conditions. As a result, it is assumed that for a given PE spectrum, the subsequent PIMS is hypothetically of the same sample.

Values of ultraviolet photoionization mass spectra (PIMS) are collected in Table 2 for the samples confirming the identity of these species. These results become more valuable when they are joined with the photoelectron spectroscopy PES and theoretical results. Table 2 shows the detected fragments using the PIMS data.

Vibrational spectra

The liquid infrared spectra in the range of 4000–400 cm^{-1} were obtained using KBr windows on the Fourier Transform Infrared (FTIR) Nexus Thermo Nicolet instrument with a resolution of 1 cm^{-1}. Furthermore, the Raman spectrum of the liquid sample was measured at room temperature using a Horiba JobinYvon T64000 Raman spectrometer between 3500 and 150 cm^{-1} with a confocal microscope and CCD detection. A Kr^{+} multiline laser with an excitation wavelength of 647.1 nm was used for the measurement. The vibrational spectra obtained from these measurements are depicted in Figure S1–S5. The observed vibrational wavenumbers

Table 2. PIMS for the species CCl_3SSR (R=CH_2CH_3, CH_2CF_3, $C(CH_3)_3$, C_6H_5, $C(O)CH_3$).

Molecule	m/z	Fragment[a]
$CCl_3SSCH_2CH_3$	29	$CH_2CH_3^{+}$
	61	$SCH_2CH_3^{+}$
	78	$SSCH_2^{+}$
	93	$SSCH_2CH_3^{+}$
	117	CCl_3^{+}
	160	$CCl_2SSCH_2^{+}$
$CCl_3SSCH_2CF_3$	46	SCH_2^{+}
	64	SS^{+}
	83	$CH_2CF_3^{+}$
	147	$SSCH_2CF_3^{+}$
	264	$CCl_3SSCH_2CF_3^{+}$
$CCl_3SSC(CH_3)_3$	27	$C(CH_3)^{+}$
	42	$C(CH_3)_2^{+}$
	57	$C(CH_3)_3^{+}$
	91	$SSC(CH_3)^{+}$
	117	CCl_3^{+}
$CCl_3SSC_6H_5$	77	$C_6H_5^{+}$
	117	CCl_3^{+}
	149	CCl_3S^{+}
$CCl_3SSC(O)CH_3$	43	$C(O)CH_3$
	60	SCO
	117	CCl_3^{+}
	154	$CClSSC(O)CH_3^{+}$

[a] Most intense isotopomer signal.

were compared with the wavenumbers computed at the B3LYP/6-311++G(3df) level of approximation of the lowest energy rotamers, and the results are listed in Table S1–S5.

Computational chemistry

Computational quantum chemistry calculations were performed using the GAUSSIAN 03 program package.[15] Density functional theory (B3LYP) was used with a basis set of 6–311++G(3df) to perform scans of the potential energy surface, structure optimizations, and vibrational wavenumbers for the CCl_3SSR compounds.[16–18] To compute the photoelectron spectra, the OVGF approach was applied with a 6–311++G(3df) basis set that includes correlation effects of the self-energy to the molecules, providing accurate results of the vertical ionization energies. Molecular orbital plots were generated using the Gauss View program with a 0.05 isodensity.

X-Ray diffraction

A single crystal of $CCl_3SSC(CH_3)_3$ was obtained and examined on a Rigaku Supernova diffractometer using MoKα ($\lambda = 0.71073$ Å) radiation at a temperature of 100.0 K. The crystal structure was solved using the ShelXT[19] structure solution program with Intrinsic Phasing, and refined using the ShelXL[20] refinement package with Least Squares minimization, using Olex2.[21] The crystal was grown in situ at 263.6 K and gradually chilled to 252 K at a rate of 1 K/h, then to 100 K at a rate of 50 K/h, resulting in oligo-crystalline material. Data reduction was performed using two domains with only a few overlapping reflections. Refinement was carried out with only one domain, which was pseudo-merohedrically twinned with a ratio of 75:25 (TWIN 1 0 0 1 −1 0 0 0 −1). The structure can also be solved and refined in *C*2/*c*, but with a disorder of the three methyl groups with the three chlorine atoms. The bond lengths and ADPs suggest a similar disorder with a small occupancy in $P\bar{1}$, but the disorder is far below the resolution of the data set and can't be refined meaningfully. Therefore, the C–C and C–Cl distances should be taken with care. Hydrogen atoms were included using a riding model. Details of the X-ray investigation are given in Table S6.

Deposition Number 2263686 (for CCl3SSC(CH3)3) contains the supplementary crystallographic data for this paper. These data are provided free of charge by the joint Cambridge Crystallographic Data Centre and Fachinformationszentrum Karlsruhe Access Structures service.

Results and Discussion

To obtain the theoretical ionization energy values of the studied species, quantum-chemical calculations were conducted using the Gaussian 03 W program with the Outer Valence Green's Function (OVGF) method. This method provides the energies associated with the valence orbitals, which depend on the molecular structure and conformation. The study of conformational equilibrium is important to determine the most stable form of the species and to understand the shape of the photoelectron spectrum.

The OVGF calculations were performed for each molecule using the optimized geometries obtained with the B3LYP/6-311++G** approximation for the lower energy conformations. Figure 1 displays the potential energy curves computed around the S–S bond for CCl_3SSR molecules (R=CH_2CH_3, CH_2CF_3, $C(CH_3)_3$, C_6H_5, $C(O)CH_3$), while Figure 2 shows the lower energy conformations and their relative energies in kcal/mol for each molecule.

$CCl_3SSCH_2CH_3$ and $CCl_3SSCH_2CF_3$ molecules show a typical *gauche* structure around the S–S bond with a dihedral angle (φ(CS–SC)/B3LYP/6-311++G**) of 93.1 and 93.4°, respectively.

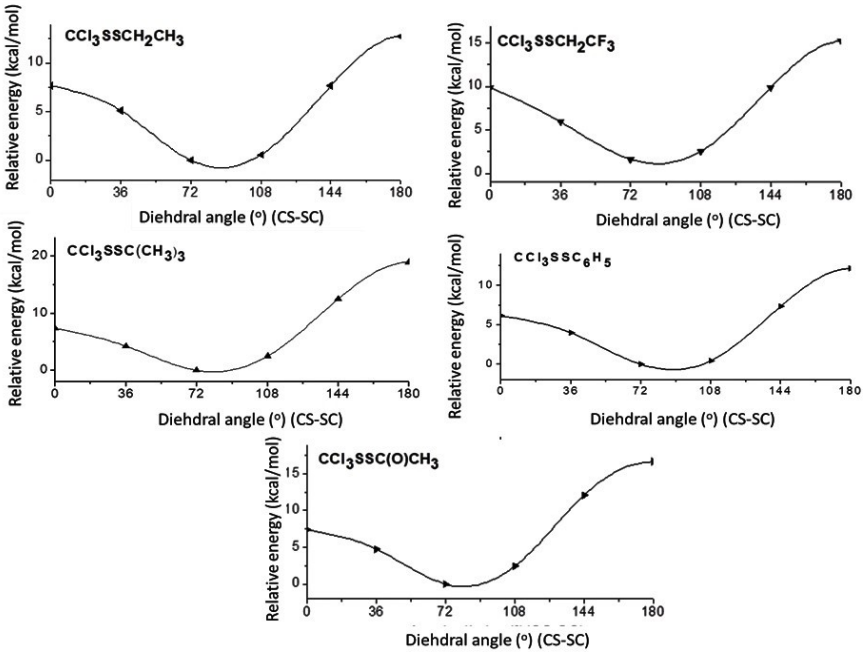

Figure 1. Potential energy curves of the CCl_3SSR molecules (R=CH_2CH_3, CH_2CF_3, $C(CH_3)_3$, C_6H_5, $C(O)CH_3$) as a function of the CS–SC dihedral angle calculated with the B3LYP/6-31++G** level of approximation.

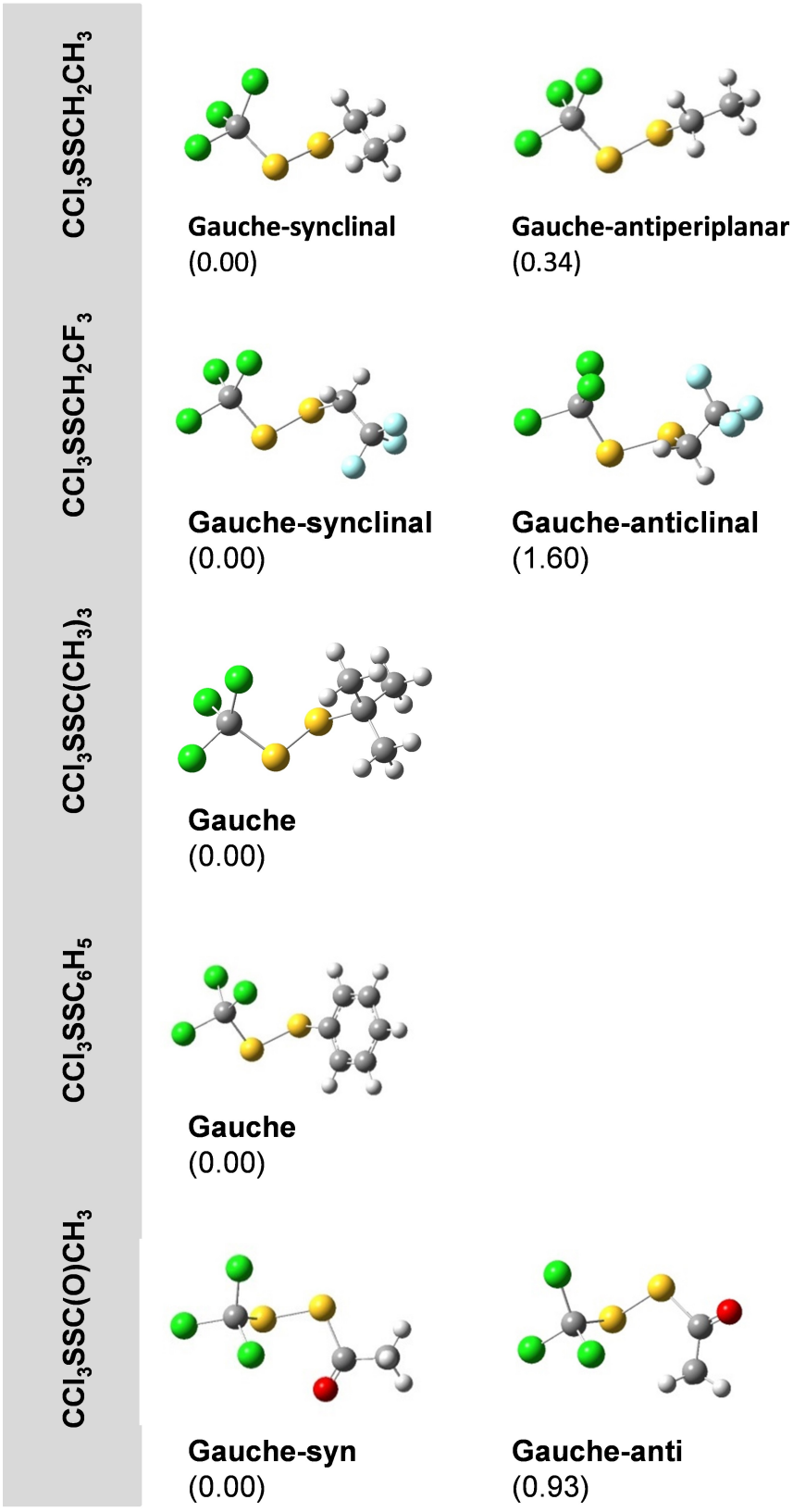

Figure 2. Lower energy rotamers and relative energies (kcal/mol) for the CCl_3SSR molecules studied in this work, calculated using the B3LYP/6-31++G** level of approximation.

A second remarkable dihedral angle involves the S–S–C–C connection, which determines the relative orientation of the C–C bond of the alkyl moiety (ethyl and trifluoroethyl) relative to the S–S bond. In both cases, the most favorable computed conformation is the synclinal with torsion angles φ(SS–CC) = 65.6 and 88.6°, while the second higher energy computed form presents an antiperiplanar conformation (φ(SS–CC) = 174.7°) for $CCl_3SSCH_2CH_3$ and anticlinal (φ(SS–CC) = −140.4°) in the case of $CCl_3SSCH_2CF_3$.

The conformation around the S–S bond for $CCl_3SSC(O)CH_3$ is as expected also *gauche*, while the lower energy form when analyzing the orientation of the carbonyl group with respect to the S–S bond, i.e. the dihedral angle φ(SS–C=O), turned out to present a synperiplanar form (φ(SS–C=O) = 2°), followed in energy by the antiperiplanarrotamer. This behavior is expected in comparison with XC(O)SY containing compounds, resulting the synperiplanar form energetically favored in all cases.[22]

A similar computational analysis computes a dihedral angle φ(CS–SC) = 90.1° for the $CCl_3SSC_6H_5$ molecule, presenting, in the same way as the previous species, a gauche conformation around the disulfide bond.

Finally, the calculation of the potential energy curve for the case of $CCl_3SSC(CH_3)_3$, located the global minimum at a dihedral angle φ(CS–SC) = 81.0°. This angle undergoes a change of several degrees when compared with the value of 107.1(2)° obtained in this work by X-ray diffraction measured in-situ for a crystal formed at low temperatures. This experimental angle is higher than the expected values for φ(CS–SC) dihedral angles in disulfides, which are close to 90°. Table 3 lists bond distances and dihedral angles calculated for this family of disulfides.

Table 3. S–S bond lengths (Å) and φ(CS–SC) torsion angles (°) for the CCl_3SSR species calculated with the B3LYP/6-311++G** approximation.

R	d(S–S) [Å]	φ(CS–SC)[°]
CH_2CH_3	2.074	93.1
CH_2CF_3	2.073	93.4
$C(CH_3)_3$	2.080 (2.0186(8))[a]	81.0 (107.1(2))[a]
C_6H_5	2.082	90.1
$C(O)CH_3$	2.053	80.5

[a]Experimental values measured in this work are between parentheses.

As can be seen, the S–S bond lengths for the molecules listed in Table 3 are in the typical range of disulfides. These distances are in the order of the values reported for the disulfides, $FC(O)SSCF_3$ (2.027(4) Å), CF_3SSCF_3 (2.030(5) Å) and CH_3SSCH_3 (2.029(3) Å) among others.[23,24] As already mentioned, the experimental value of 107.1(2)° found for $CCl_3SSC(CH_3)_3$ is notoriously larger for this type of compound where an angle near to 90° would be expected. This fact could be mainly attributed in the present case to the steric factor caused by the bulky tert-butyl group.

Low temperature crystal structure of $CCl_3SSC(CH_3)_3$

$CCl_3SSC(CH_3)_3$ adopts the triclinic system belonging to the space group $P\bar{1}$. It shows two molecules per unit cell and cell parameters a = 6.0302(2) Å, b = 8.8045(2) Å, c = 10.3566(3) Å and α = 75.643(2)°, β = 89.827(2)° and γ = 70.003(2)° with a cell volume of V = 498.55(3) Å.[3] The structure was refined with 2936 independent reflections, 2820 reflections with $I > 2\sigma(I)$. Figure 3 represents the refined structure for $CCl_3SSC(CH_3)_3$ whereas Figure 4 depicts its corresponding packing motif. The complete crystallographic information can be found in Tables S6 in the Supplementary Information.

Selected experimental and computed (B3LYP/6-311++G**) geometric parameters (distances in Å, angles in degrees) for the lowest energy form of $CCl_3SSC(CH_3)_3$ are listed in Table 4.

Two types of intermolecular interactions are present in the crystal (Figure 4, on the right side), the S1···Cl2 of neighbor molecules and Cl3···Cl3. Their distances are, respectively, 3.415(1) and 3.363(1) Å lower than the sum of the van der Waals radii of 3.55 and 3.50 Å. As determined in the study of the origin of these effects in the crystal, both the Cl3···Cl3 C1 halogen bond with 167.0(1)° and the S1···Cl2 C1 with 172.0(1)° tend to present a linear geometry.[25,26]

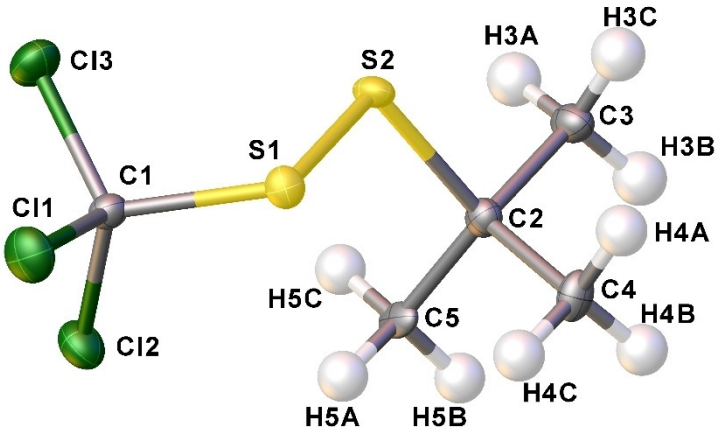

Figure 3. Refined crystal structure of $CCl_3SSC(CH_3)_3$ (with the exception of hydrogen atoms, the displacementprobability of thethermalellipsoids are 50%).

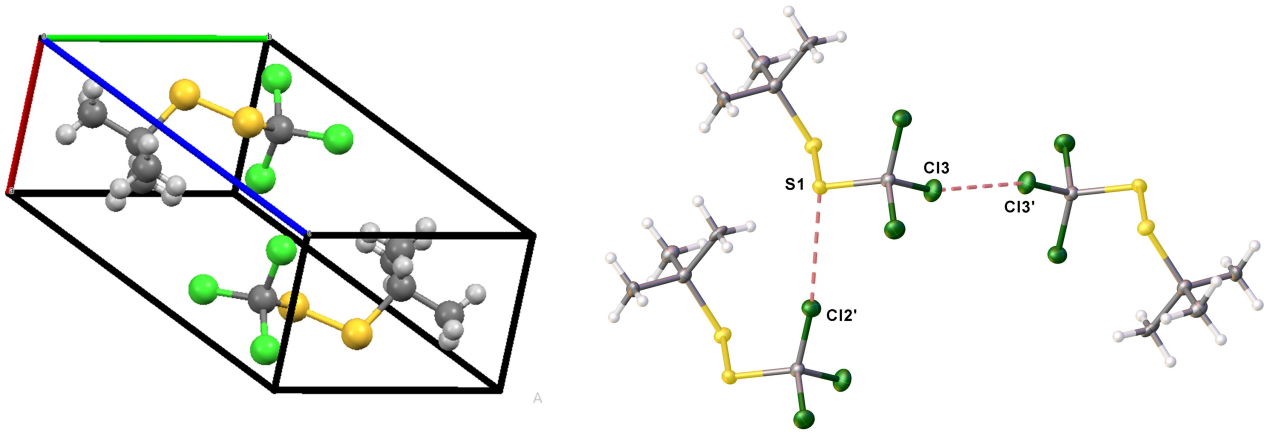

Figure 4. Two views of the packing structures for $CCl_3SSC(CH_3)_3$. The *a*, *b* and *c* cell parameters are colored in red, green and blue, respectively. The intramolecular interactions of S1···Cl2′(1 + x,y,z,) with 3.415(1) Å and Cl3···Cl3′(2−x,−y,2−z) with 3.363(1) Å can be evidenced on the right side of this Figure.

Table 4. Selected geometrical parameters of crystalline $CCl_3SSC(CH_3)_3$ obtained by an in-situ crystallization method.

Parameter[a]	Bond length	Parameter[a]	Bond angle [°]
Cl1–C1	1.778(3)	C1–S1–S2	106.24(9)
Cl2–C1	1.775(3)	C2–S2–S1	107.35(9)
Cl3–C1	1.760(3)	Cl1–C1–S1	103.04(14)
S1–S2	2.0186(8)	Cl2–C1–Cl1	108.63(15)
S1–C1	1.834(3)	Cl2–C1–S1	114.22(14)
S2–C2	1.861(3)	Cl3-C1-Cl1	109.75(14)
C2–C3	1.599(4)	Cl3–C1–Cl2	108.59(15)
C2–C4	1.578(4)	Cl3–C1–S1	112.40(15)
C2–C5	1.584(4)	C3–C2–S2	101.98(17)
		C4–C2–S2	111.38(18)
		C4–C2–C3	111.0(2)
		C4–C2–5	110.8(2)
		C5–C2–S2	111.65(16)
		C5–C2–C3	109.7(2)
		C1–S1–S2–C2	107.1(2)

[a] See Figure 3 for the atomic numbers.

Vibrational spectra

Experimental FTIR and Raman spectra were measured for these species in the liquid phase. Vibrational wavenumbers derived from computational approaches are also included in Table S1–S5. Table 5 summarizes the experimental wavenumbers whose modes are characteristic of the CCl_3SS– moiety for each CCl_3SSR (R═CH_2CH_3, CH_2CF_3, $C(CH_3)_3$, C_6H_5, $C(O)CH_3$) molecule.

The FTIR spectra are characterized by very intense absorptions in the 800–750 cm^{-1} region assigned to the antisymmetrical and symmetrical stretching vibrational modes of the perchloromethyl group, ν_{as} (CCl_3) and ν_s (CCl_3). The S–S stretching vibrational mode appears as weak intensity bands in the FTIR spectrum but of considerable intensity in the Raman spectra, observed in the 500 cm^{-1} region. The ν(S–CCl_3) vibrational stretching mode is observed in all cases as a very and low intense Raman and FTIR bands, respectively, with values close to 440 cm^{-1}. These data are in good agreement with the values reported for relevant examples found in the literature as CCl_3SCl[27] and for the molecules $CCl_3SOC(O)CH_3$[28] and $ClC(O)OCCl_3$.[29]

The vibrational behavior of the S–S bond has been interpreted from different perspectives, including differences in the degree of substitution at the β carbons in a CCl_3S–S–C^{β}–C^{α}

Table 5. FTIR and Raman vibrational wavenumbers of the CCl_3SSR species studied in this work.

Vibrational mode	R═				
	–CH_2CH_3[a]	–CH_2CF_3[b]	–$C(CH_3)_3$[a]	–C_6H_5[a]	–$C(O)CH_3$[a]
ν_{as} (CCl_3)	785.6	722.9	785.9	786.5/**787.2**	790.3
ν_{as} (CCl_3)	754.6	696.1	754.2/**758.4**	762.2/**765.9**	763.6
ν_s (CCl_3)	743.0	683.4	733.5/**735.7**	741.3/**742.5**	748.0
ν (S–C(R))	574.5	607.3	572.2/**563.5**	685.8/**694.6**	515.5/**532.5**
ν (S–S)	526.5/**527.1**	507.4	547.1/**540.9**	483.9/**481.8**	537.5/**546.3**
ν (S–CCl_3)	441.3/**442.3**	503.5	441.0/**440.7**	440.9/**440.3**	461.5/**461.7**

[a] The bold signal corresponds to the Raman spectrum.
[b] From the B3LYP/6-311 + + g(d,p) level of approximation.

unit and differences in conformation around their S–S bonds.[30] The correlation between the S–S wavenumber and the sum of the substituent electronegativities bonded to the S–S group has also been analyzed.[31] In all cases, it should be noted that the S–S internal coordinate does not correspond to a single normal mode, which means that it is not linked to a specific wavenumber or vibrational transition. A holistic way to estimate the partial contribution of the S–S stretching to the corresponding normal mode of vibration is to calculate the potential energy distribution of each of the internal coordinates that contribute to the normal mode.

Adopting the Wilson method and solving the equation źGF–λE, a particular wavenumber can be linked to the F and G matrices. The F matrix is the force constants matrix, which introduces the vibrational potential energy. The G matrix is the matrix for the contribution of the masses and spatial relationships of the atoms in the molecule, which introduces the kinetic energy in the procedure. E is the unit matrix and λ introduces the value of the squared wavenumber into the equation.

NMR spectra

Table 1 shows experimental and calculated ^{1}H NMR, ^{13}C NMR chemical shifts for the CCl_3SSR species with R═CH_2CH_3, CH_2CF_3, $C(CH_3)_3$, C_6H_5 and $C(O)CH_3$,and their comparison with the calculated monosulfide analogs. For the only fluorinated species, $CCl_3SSCH_2CF_3$, the experimental ^{19}F NMR was also measured. Analyzing the ^{13}C NMR chemical shifts for the first aliphatic species belonging to both the CCl_3SR and the CCl_3SSR series it is observed higher chemical shifts for the C^{β}linked to the S–S bridge. For cysteine and cystine the experimental reported ^{13}C NMR chemical shifts are 28.4 ± 2.4 and 40.7 ± 3.8.[32] Thetendency of the calculated values agrees reasonably well with these experimental data being 25.8 and 37.4, respectively, for the species in their neutral form. This behavior was also observed for a number of cysteine and cysteine amino acids. The general trend is that the C^{β}shifts for the reduced cysteines is lower than the corresponding value for the oxided S–S cystines.[32]

Photoelectron spectra

As already mentioned in the experimental part, the photoelectron spectra in the gaseous phase were measured with a UPS-II camera equipment that uses a helium lamp of 21.21 eV energy (HeI) as a radiation source. According to the Franck-Condon principle, the most probable and intense transition between the fundamental and ionized states corresponds to the vibrationally excited state of the positive ion that has the same geometry as the neutral molecule. This transition is referred to as the "vertical" ionization energy. Adiabatic ionization energies, on the other hand, take into account the relaxation of the remaining electrons in the molecule after the electron is removed and refer to the minimum energy required to remove an electron from a molecule or atom in its ground state to produce a cation in its ground state. Since for compounds containing sulfur atoms, the Franck-Condon factors are low near the absorption edges, which mean that the relaxation process occurs too slowly for the system to remain in a single electronic state. Therefore, adiabatic ionization energies of sulfur compounds cannot be obtained using standard photoelectron spectroscopy techniques.

Figure S6 shows the gas phase photolectron spectra for the CCl_3SSR series (R═CH_2CH_3, CH_2CF_3, $C(CH_3)_3$, C_6H_5, $C(O)CH_3$). For better observation and comparison of the results, a correlation scheme for the lowest ionization energies for the measured molecules was built, as shown in Figure 5.

Table 6 shows the comparative experimental and theoretical results of the series of perchloromethyl disulfide compounds. With the exception of $CCl_3SSC_6H_5$, the first two ionization energies correspond to nonbonding electrons located on the sulfur atoms of the disulfide bond. The results obtained from quantum chemical calculations showed little variation between these two values and satisfactorily predicted the experimental values.

The experimental ionization energy data agree with reported values for similar disulfides, such as CH_3SSCH_3[33] and *t*-Bu–SS-*t*-Bu,[34] with values of 8.98 and 8.14 eV, respectively. On the other hand, the photoelectron spectrum reported for thioacetic acid and its derivative, the ethyl thioacetic thioester, show the presence of two signals at 10.06 and 10.30 eV ($CH_3C(O)SH$) and 9.44 and 9.65 eV ($CH_3C(O)SCH_2CH_3$), respectively, due to the ionization processes originated in the nonebonding electron pairs attached the sulfur (π) and oxygen atoms of the carbonyl bond.[35]

As pointed out by Baker et al.,[36] the first two bands in the photoelectron spectrum of disulfides correspond to the symmetric and antisymmetric linear combinations of the outermost p-atomic orbitals. The splitting observed in disulfide compounds is generally explained by the so-called Walsh diagrams,[37] which account for the interaction between the free pairs of adjacent sulfur atoms and their dependence on the variation of the dihedral angle around the –SS– bond.[38] While in the fundamental neutral state of symmetrically substituted disulfides the non-bonding orbitals of the sulfur atoms, corresponding to HOMO orbitals, are nearly degenerate, after ionization this degeneracy is removed due to the change in the geometry of the cation, giving rise to the observed splitting in the photoelectron spectra. Although this explanation has the advantage of being qualitative and satisfactory, it is not appropriate for asymmetrically substituted disulfides, for which a degeneracy of the free pairs of the sulfur atoms cannot be a priori guaranteed for the equilibrium position of the dihedral angle. In case of asymmetrically substituted disulfides, theoretical calculations explain this splitting as an energetic difference between the free sulfur pairs, due to the different nature of the substituents attached to each of them.

It is clear that the substitution of the hydrogen atoms by more electronegative groups in the HSSH[39] leads to an increase in the ionization energy values of the substituted disulfides, while the replacement by electron donor groups produces the opposite effect. This behavior is observed in a variety of cases

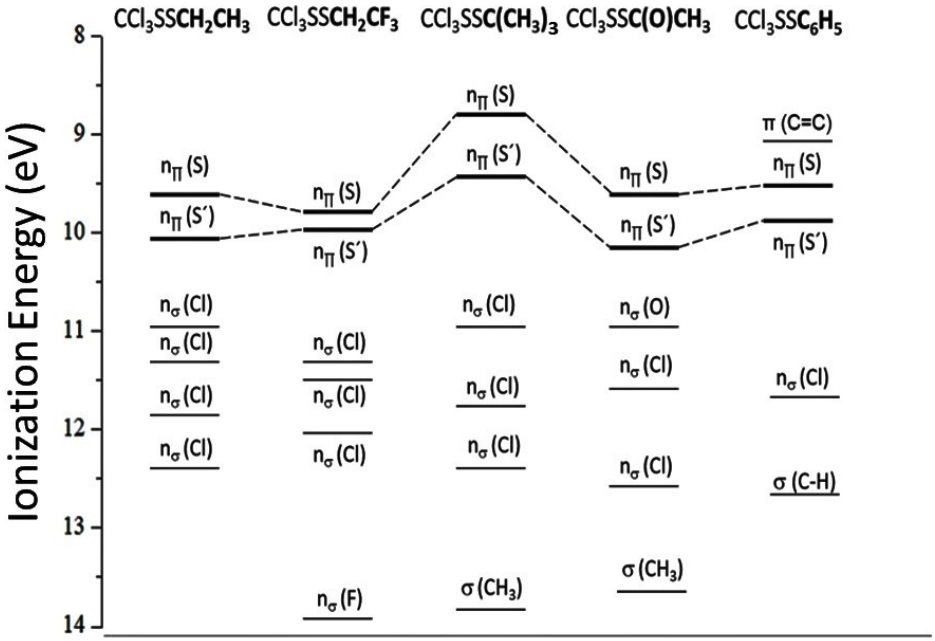

Figure 5. Schematic representation of the experimental energies of the outermost orbitals of the CCl_3SSR species (R═CH_2CH_3, CH_2CF_3, $C(CH_3)_3$, $C(O)CH_3$ and C_6H_5).

Table 6. Values of the first two ionization energies for perchloromethyl disulfides CCl_3SSR.

Molecule	IonizationEnergy(IE)				MO	Assignment
	EI [eV]	ΔE[a]	Calculated[b]	φ[°][c]		
$CCl_3SSCH_2CH_3$	9.58	0.52	9.24	93.1	53	Lpπ S(Et)
	10.10		9.41		52	Lpπ S(CCl_3)
$CCl_3SSCH_2CF_3$	9.80	0.19	9.79	93.4	65	Lpπ S(Et)
	9.99		9.92		64	Lpπ S(CCl_3)
$CCl_3SSC(CH_3)_3$	8.86	0.59	8.72	81.0	61	Lpπ S(tert-but)
	9.45		9.46	**107.1**[d]	60	Lpπ S(CCl_3)
$CCl_3SSC_6H_5$	9.04		8.74	90.1	65	π(C═C) Ph
			9.32		63	
	9.51	0.33*	9.37		62	Lp π S(Ph)
	9.84		9.65		61	Lp π S(CCl_3)
$CCl_3SSC(O)CH_3$	9.60	0.60	9.50	80.5	56	Lpπ S(CCl_3)
	10.20		9.97		55	Lpπ S(C═O)

[a] △E═EI1−EI2,
[b] Calculated at the OVGF/6-311 + + G** level of the theory,
[c]Torsion angle CSSC corresponding to the most stable conformation and
[d] experimental value measured in this work. Lp: "lone pair". *corresponding to △E═EI2−EI3.

reported in the literature for molecules with electron-withdrawing groups, such as $FC(O)SSCH_3$[40] and CCl_3SSCN.[41] For the present case, for instance, the first ionization energy of $CCl_3SSCH_2CH_3$ is 9.58 eV while for its fluorinated analog, $CCl_3SSCH_2CF_3$, the value is 9.80 eV. In general, as it can be seen in Table 6, the non-bonding electron pair with the lower ionization value corresponds to the sulfur atom bounded to the different substituent groups. The *tert*-butyl trichloromethyl disulfide presents ionization energy of 8.86 eV showing the lowest ionization energy of this series. This might be expected according to the "donor" effect of the alkyl groups ($C(CH_3)_3 < C_6H_5 < CH_2CH_3 < C(O)CH_3 < CH_2CF_3$). The ionization energies are therefore decreasing as the donor character of the substituent group increases. Thus, the non-bonded electron pair at the sulfur atom attached to the "acceptor" group CCl_3 presents higher ionization energy with ionization energies varying in a much more limited range. This general behavior was also studied for a series of −SCN containing molecules.[42]

Conclusions

In this work syntheses of a series of trichloromethyl disulfide compounds CCl_3SSR, with R=CH_2CH_3, CH_2CF_3, $C(CH_3)_3$, $C(O)CH_3$ and C_6H_5, are presented. They were identified and suitably characterized by nuclear magnetic resonance techniques and vibrational spectroscopy. Using FTIR and Raman spectroscopy techniques, the most intense signals of the liquid phase spectra were characterized and the vibration modes were assigned with the help of quantum-chemical calculations and by the comparison with related species.

All the molecules in the neutral state showed a gauche conformational preference around the dihedral angle φ(CSSC). This was experimentally reconfirmed in the case of the $CCl_3SSC(CH_3)_3$ molecule with X-ray diffraction measurements at low temperatures. The structure presents an experimental angle value equal to $\varphi(CSSC) = 107.1(2)^\circ$. The introduction of the sterically demanding *tert*-butyl group clearly affects the structure around the central disulfide bond, with the largest value of the φ(CSSC) dihedral angle on the whole series of studied disulfides. In addition, it was found that the molecules is stabilized in the crystal with interactions of the C–S···Cl and C–Cl···Cl type.

The highest value of 9.80 eV found for the ionization energy of the compound belonging to this series corresponds to the ionization of an electron formally located at a non-bonded free orbital of the sulfur atom linked with the carbon atom in the $CCl_3SSCH_2CF_3$ molecule, while the lowest with a value of 8.86 eV corresponds to the equivalent ionization when R=$C(CH_3)_3$.

In conclusion, further evidence is provided for the significant impact of substituents on the molecular structure and electronic distribution of asymmetric disulfides. Our findings demonstrate that this effect is largely mediated by the steric as well as the donor/withdrawal properties of the substituents. This behavior can be extrapolated to other disulfides, which may have implications in the origin of life and, conversely, in processes connected to COVID-19.

Supporting Information Summary

The Supporting Information includesexperimental (FTIR y Raman) and computed wavenumbers (B3LYP/6-311++G**) of $CCl_3SSCH_2CH_3$ (Table S1), computed wavenumbers (B3LYP/6-311++G**) of $CCl_3SSCH_2CF_3$(Table S2), Experimental (FTIR and Raman) and computed wavenumbers (B3LYP/6-311++G**) of $CCl_3SSC(O)CH_3$(Table S3), $CCl_3SSC(CH_3)_3$ (Table S4), and $CCl_3SSC_6H_5$ (Table S5), crystal data and structure refinement for $CCl_3SSC(CH_3)_3$ (Table S6), ^{1}H(Figure S1) and^{13}C(Figure S2) NMR spectra of $CCl_3SSCH_2CH_3$, ^{1}H (Figure S3),^{13}C (Figure S4) and ^{19}F(Figure S5) NMR spectra of $CCl_3SSCH_2CF_3$, ^{1}H (Figure S6) and^{13}C (Figure S7) NMR spectra of$CCl_3SSC(CH_3)_3$, ^{1}H (Figure S8) and ^{13}C (Figure S9) NMR spectra of$CCl_3SSC_6H_5$, ^{1}H (Figure S10) and ^{13}C (Figure S11) NMR spectra of$CCl_3SSC(O)CH_3$, FTIR and Raman spectra of liquid $CCl_3SSCH_2CH_3$ (Figure S12), calculated FTIR spectrum of $CCl_3SSCH_2CF_3$ (Figure S13), FTIR and Raman spectra of liquid $CCl_3SSC(O)CH_3$ (Figure S14), $CCl_3SSC(CH_3)_3$ (Figure S15), and $CCl_3SSC(O)C_6H_5$ (Figure S16), Photoelectron spectra for the species CCl_3SSR, (R=CH_2CH_3, CH_2CF_3, $C(CH_3)_3$, C_6H_5, $C(O)CH_3$) (Figure S17).

Acknowledgements

Theauthorsfrom Argentina acknowledgethe Consejo Nacional de Investigaciones Científicas y Técnicas (CONICET) (PIP 0352 and PUE-2017-22920170100053), the Agencia Nacional de Promoción Científica y Tecnológica (ANPCyT) (PICT-2018-04355 and PICT-2020-03746), the Comisión de Investigaciones Científicas de la Provincia de Buenos Aires (CIC), and the Facultad de Ciencias Exactas, UNLP (UNLP-X822) forprovidingfinancialsupport. MFE, RMR, and CODV acknowledge the Chinese Academy of Sciences for funding their stay at the Laboratory of MFG in Beijing. VMC and C.O.D.V. express their gratitude to the Lehrstuhl für Anorganische Chemie und Strukturchemie, Bielefeld University, for providing financial support that allowed V.M.C. to stay in Germany. Open Access funding enabled and organized by Projekt DEAL.

Conflict of Interests

The authors declare no conflict of interest.

Data Availability Statement

The data that support the findings of this study are available from the corresponding authors upon reasonable request.

Keywords: Disulfides · Crystal structure · Conformation · Photoelectron spectroscopy · Electronic structure

[1] C. W. Scheele, *Chemische Abhandlung von der Luft und dem Feuer*, Published by Magn. Swederus, bookseller **1777**, p. 162.
[2] G. Pelz, K. M. T. Yamada, G. Winnewisser, *J. Mol. Spectrosc.* **1993**, *159*, 507–520.
[3] J. Trost, K. Hornberger, *Phys. Rev. Lett.***2009**,*103*, 23202-1/4.
[4] C. Day, *Phys. Today* **2009**, *62*, 16–17.
[5] G. Wächtershäuser, *Philos. Trans. R. Soc. London Ser. B* **2006**, *361*, 1787–1808.
[6] F. A. Kundell, *Origins Life Evol. Biospheres* **2011**, *41*, 175–198.
[7] P. J. Hogg, *Trends Biochem. Sci.* **2003**, *28*, 210–214.
[8] M. Góngora-Benítez, J. Tulla-Puche, F. Albericio, *Chem. Rev.* **2014**, *114*, 901–926.
[9] S. J. Brois, J. F. Pilot, H. W. Barnum, *J. Am. Chem. Soc.* **1970**, *92*, 7629–7631.
[10] E. Mühlbauer, W. Weiss, *DE 1219925*, *Bayer AG***1965**.
[11] D. Banfi, L. Patiny, *Chimia* **2008**, *62*, 280–281.
[12] A. M. Castillo, L. Patiny, J. Wist, *J. Magn. Reson.* **2011**, *209*, 123–130.
[13] J. Aires-de-Sousa, M. C. Hemmer, J. Gasteiger, *Anal. Chem.* **2002**,*74*, 80–90.
[14] Z. Sun, S. J. Zheng, J. Wang, X. J. Zhu, M. F. Ge, D. X. Wang, *Chem. Eur. J.* **2001**, *14*, 2995–2999.
[15] M. J. Frisch, G. W. Trucks, H. B. Schlegel, G. E. Scuseria, M. A. Robb, J. R. Cheeseman, J. A. Montgomery Jr., T. Vreven, K. N. Kudin, J. C. Burant, J. M. Millam, S. S. Iyengar, J. Tomasi, V. Barone, B. Mennucci, M. Cossi, G. Scalmani, N. Rega, G. A. Petersson, H. Nakatsuji, M. Hada, M. Ehara, K. Toyota, R. Fukuda, J. Hasegawa, M. Ishida, T. Nakajima, Y. Honda, O.

Kitao, H. Nakai, M. Klene, X. Li, J. E. Knox, H. P. Hratchian, J. B. Cross, V. Bakken, C. Adamo, J. Jaramillo, R. Gomperts, R. E. Stratmann, O. Yazyev, A. J. Austin, R. Cammi, C. Pomelli, J. W. Ochterski, P. Y. Ayala, K. Morokuma, G. A. Voth, P. Salvador, J. J. Dannenberg, V. G. Zakrzewski, S. Dapprich, A. D. Daniels, M. C. Strain, O. Farkas, D. K. Malick, A. D. Rabuck, K. Raghavachari, J. B. Foresman, J. V. Ortiz, Q. Cui, A. G. Baboul, S. Clifford, J. Cioslowski, B. B. Stefanov, G. Liu, A. Liashenko, P. Piskorz, I. Komaromi, R. L. Martin, D. J. Fox, T. Keith, M. A. Al-Laham, C. Y. Peng, A. Nanayakkara, M. Challacombe, P. M. W. Gill, B. Johnson, W. Chen, M. W. Wong, C. Gonzalez, J. A. Pople, *Gaussian*, Inc., Wallingford CT **2004**.
[16] A. D. Becke, *J. Chem. Phys.* **1993**, *98*, 5648–5652.
[17] C. Lee, W. Yang, R. G. Parr, *Phys. Rev. B* **1988**, *37*, 785–789.
[18] J. P. Perdew, K. Burke, M. Ernzerhof, *Phys. Rev. Lett.* **1996**, *77*, 3865–3868.
[19] G. M. Sheldrick, *Acta Crystallogr. Sect. A* **2015**, *71*, 3–8.
[20] G. M. Sheldrick, *Acta Crystallogr. Sect. C* **2015**, *71*, 3–8.
[21] O. V. Dolomanov, L. J. Bourhis, R. J. Gildea, J. A. K. Howard, H. Puschmann, *J. Appl. Crystallogr.* **2009**, *42*, 339–341.
[22] V. M. Cayón, M. F. Erben, R. M. Romano, H.-G. Stammler, N. W. Mitzel, C. O. Della Védova, *New J. Chem.* **2020**, *44*, 14568–14577.
[23] A. Hermann, S. E. Ulic, C. O. Della Védova, H.-G. Mack, H. Oberhammer, *J. Fluorine Chem.* **2001**, *112*, 297–305.
[24] S. Torrico-Vallejos, M. F. Erben, R. Boese, C. O. Della Védova, *New J. Chem.* **2010**, *34*, 1365–1372.
[25] P. Scilabra, G. Terraneo, G. Resnati, *Acc. Chem. Res.* **2019**, *52*, 1313–1324.
[26] G. Cavallo, P. Metrangolo, R. Milani, T. Pilati, A. Priimagi, G. Resnati, G. Terraneo, *Chem. Rev.* **2016**, *116*, 2478–2601.
[27] C. O. Della Védova, P. J. Aymonino, *J. Raman Spectrosc.* **1986**, *17*, 485–486.
[28] M. Cuaquira-Reina, R. Boese, M.-F. Ge, S. E. Ulic, H. Beckers, H. Willner, C. O. Della Védova, *J. Phys. Chem. A* **2008**, *112*, 7939–7946.
[29] V. B. Arce, C. O. Della Védova, A. J. Downs, S. Parsons, R. M. Romano, *J. Org. Chem.* **2006**, *71*, 3423–3428.
[30] H. E. Van Wart, H. A. Scheraga, *J. Phys. Chem.* **1976**, *80*, 1823–1832.
[31] C. O. Della Védova, *J. Raman Spectrosc.* **1989**, *20*, 279–282.
[32] D. Sharma, K. Rajarathnam, *J. Biomol. NMR* **2000**, *18*, 165–171.
[33] H. Bock, G. Wagner, *Angew. Chem.* **1972**, *84*, 119–120.
[34] M.-F. Guimon, C. Guimon, G. Pfister-Guillouzo, *Tetrahedron Lett.* **1975**, *16*, 441–444.
[35] K. Watanabe, T. Nakayama, J. Mottl, *J. Quant. Spectrosc. Radiat. Transfer* **1962**, *2*, 369–382.
[36] A. D. Baker, M. Brisk, M. Gellender, *J. Electron Spectrosc. Relat. Phenom.* **1974**, *3*, 227–228.
[37] A. D. Walsh, *J. Chem. Soc.* **1953**, 2288–2296.
[38] K. Kimura, K. Osafune, *Bull. Chem. Soc. Jpn.* **1975**,*48*, 2421–2427.
[39] B. Solouki, H. Bock, *Inorg. Chem.* **1977**,*16*, 665–669.
[40] M. F. Erben, C. O. Della Védova, *Inorg. Chem.* **2002**,*41*, 3740–3748.
[41] L. Du, L. Yao, M.-F. Ge, *Chin. J. Chem. Phys.* **2008**,*21*, 93–99.
[42] L. S. Rodríguez Pirani, C. O. Della Védova, M. Geronés, R. M. Romano, R. Cavasso-Filho, M.-F. Ge, C. Ma, M. F. Erben, *J. Phys. Chem. A* **2017**,*121*, 9201–9210.

Manuscript received: July 1, 2023